

Moiré Engineering and Topological Flat Bands in Twisted Orbital-Active Bilayers

Huan Wang,¹ Yadong Jiang,¹ Zhaochen Liu,¹ and Jing Wang^{1,2,3,*}

¹State Key Laboratory of Surface Physics and Department of Physics, Fudan University, Shanghai 200433, China

²Institute for Nanoelectronic Devices and Quantum Computing, Fudan University, Shanghai 200433, China

³Zhangjiang Fudan International Innovation Center, Fudan University, Shanghai 201210, China

(Dated: September 15, 2022)

Topological flat bands at the Fermi level offer a promising platform to study a variety of intriguing correlated phase of matter. Here we present band engineering in the twisted orbital-active bilayers with spin-orbit coupling. The symmetry constraints on the interlayer coupling that determines the effective potential for low-energy physics of moiré electrons are exhaustively derived for two-dimensional point groups. We find the line graph or biparticle sublattice of moiré pattern emerge with a minimal C_3 symmetry, which exhibit isolated electronic flat bands with nontrivial topology. The band flatness is insensitive to the twist angle since they come from the interference effect. Armed with this guiding principle, we predict that twisted bilayers of 2H-PbS₂ and CdS realize the salient physics to engineer two-dimensional topological quantum phases. At small twist angles, PbS₂ heterostructures give rise to an emergent moiré Kagomé lattice, while CdS heterostructures lead to an emergent moiré honeycomb lattice, and both of them host moiré quantum spin Hall insulators with almost flat topological bands. We further study superconductivity of these two systems with local attractive interactions. The superfluid weight and Berezinskii-Kosterlitz-Thouless temperature are determined by multiband processes and quantum geometry of the band in the flat-band limit when the pairing potential exceeds the band width. Our results demonstrate twisted bilayers with multi-orbitals as a promising tunable platform to realize correlated topological phases.

Introduction. Recently twisted van der Waals heterostructures are becoming a novel tunable platform to realize various intriguing electronic phases in two dimensions [1–5]. Two prime examples are twisted graphene and transition metal dichalcogenide (TMD) multilayers, where correlated insulation, superconductivity and interaction-induced quantum anomalous Hall effect have been discovered [6–20]. These interesting phenomena stem from the quenched kinetic energy due to quantum interference effect in the moiré superlattice, where strong electron interaction dominates in the almost dispersionless bands near or at the Fermi level [21–24]. The highly tunable twist angle and gate provide experimental access to study the paradigmatic models of strongly-correlated electrons [4]. However, the band width of the almost flat bands in twisted graphene multilayers varies rapidly with the twist angle, which poses the main experimental difficulty requiring the angle precision to be better than 0.1° in order to achieve the band flatness [6]. Moreover, the superfluid weight is bounded when the flat band is topological [25–32], which could increase the superconducting critical temperature. Heuristically, topological bands contain extended states with algebraically decaying tails [33], which participate in the superconductivity [34–36]. Therefore, it is important to find a topological moiré system, wherein the quasiflat bands have topological properties and its band width is insensitive to twist angle.

It is well known that the flat bands exist in the line and split graph of biparticle lattices [37–44]. These bands have been exhaustively predicted in stoichiometric materials [45, 46]. However, the crystalline materials with isolated topological flat bands are still lacking. The pre-

vious studies have shown that new lattice structure and effective orbitals will emerge after twist in the moiré pattern, for example the Γ -valley TMD moiré bands [47, 48] and magnetic moiré surface bands in topological insulators [49, 50]. There, a two-orbital model on a honeycomb lattice and a single-orbital model on a Kagomé lattice emerge from the Γ -valley moiré bands, which exhibit flat bands in their spectra. However, these flat bands are gapless due to absence of spin-orbit coupling (SOC). In this work, we present the topological moiré engineering in the twisted orbital-active bilayers with SOC, and predict isolated flat bands with nontrivial topology guaranteed by certain symmetries. We further propose two candidate materials 2H-PbS₂ and CdS to demonstrate the topological flat bands near or at the Fermi level, opening up an exotic regime for experimental and theoretical investigation. Finally, we study superconductivity in these systems with local attractive interactions.

Twisted multi-orbital bilayer. We present the moiré engineering by starting from the twisted bilayer with generic multi-orbitals in each layer, which naturally exhibit atomic SOC. We consider stacking of two identical layers with the z axis as a normal direction. The angle mismatch is achieved when rotating the upper layer and the lower layer by $+\varphi/2$ and $-\varphi/2$ around the z axis, respectively. \mathbf{a}_1 and \mathbf{a}_2 are the Bravais unit vectors of each layer. Now the twist leads to the moiré pattern with periodicity of \mathbf{L}_1 and \mathbf{L}_2 as

$$\mathbf{L}_i = -\frac{\hat{z} \times \mathbf{a}_i}{2 \sin(\varphi/2)}. \quad (1)$$

The system is locally well approximated by an untwisted bilayer in a small-angle limit, while globally the moiré

symmetry group	C_3	C_{3v}	C_4	C_{4v}	C_6	C_{6v}
base momentum \mathbf{k}_0	Γ	Γ	Γ, M	Γ, M	Γ	Γ
multi-orbitals ℓ_z	± 1	± 1	± 1	± 1	± 1 or ± 2	± 1 or ± 2

TABLE I. The two-dimensional point groups with 2d irreducible representation for the spinless case under time-reversal symmetry. The angular momentum ℓ_z can be from atomic orbitals as well as the lattice.

pattern is described by spatial modulation in the stacking condition. The generic effective model for such a system under the influence of the moiré pattern is written as

$$H_{\text{eff}} = \begin{pmatrix} H_u(-i\nabla) & V(\mathbf{r}) \\ V^\dagger(\mathbf{r}) & H_l(-i\nabla) \end{pmatrix}, \quad (2)$$

where the diagonal terms $H_{u,l}(-i\nabla)$ are the kinetic energy in upper and lower layer with the twist angle $\pm\varphi/2$, and the off-diagonal term $V(\mathbf{r})$ is the interlayer coupling, i.e., the moiré potential, which depends on the local stacking condition. The stacking is described by in-plane relative shift of the two layers, $\mathbf{t}(\mathbf{r}) \equiv \mathbf{t}_u(\mathbf{r}) - \mathbf{t}_l(\mathbf{r})$, where $\mathbf{t}_{u/l}(\mathbf{r}) = \pm \sin(\varphi/2)\hat{z} \times \mathbf{r}$. The origin $\mathbf{t} = 0$ corresponds to the upper layer right-on-top of the lower layer, i.e., vertical shift. $V(\mathbf{r})$ depends on position through the spatial dependence of $\mathbf{t}(\mathbf{r})$. In the small-angle limit, $H_{u/l}$ containing spatial derivative becomes less important and $V(\mathbf{r})$ dominates. As such, we treat $H_{u/l}$ as perturbation, and diagonalize H_{eff} with only the off-diagonal components [51–53]. We can see the diagonalized $V(\mathbf{r})$ plays a role of potential energy, and its extremum could trap band electrons and may form new lattice structure. Therefore knowing the properties of $V(\mathbf{r})$ is important to understand the electronic structure in twisted bilayers.

Central to the present work, we consider the multi-orbitals in each layer and require each layer to have quadratic band dispersion, which is different from that in twisted graphene and TMD bilayer. Thus when SOC is neglected, the Fourier transformation of $H(-i\nabla)$ is degenerate at the *base momentum* \mathbf{k}_0 and lowest $\mathbf{k} \cdot \mathbf{p}$ expansion around it is $\delta\mathbf{k}^2$, i.e., quadratic band touching. The little group of \mathbf{k}_0 must be high symmetry. Table I lists all of the possible planar point groups with 2d irreducible representation for the spinless case, the corresponding base momentum and angular momentum ℓ_z of degenerate multi-orbitals. We assume that each layer has the full symmetry of that in Table I. Now the emergent moiré lattice is determined by $V(\mathbf{r})$, whose concrete form is constrained by the corresponding symmetry [54]. Here we demonstrate $V(\mathbf{r})$ and emergent moiré lattice for the typical C_{6v} here, and relegate the detailed calculation for the symmetry groups in Table I in Supplementary Materials.

Effective model and emergent lattice. For the degenerate orbitals with $\ell_z = \pm 1$, the $\mathbf{k} \cdot \mathbf{p}$ model of electronic

state in each layer with C_{6v} symmetry at Γ point is

$$H_{\text{single}}(\mathbf{k}) = -\frac{\hbar^2}{2m^*} \{ (k_x^2 + k_y^2) \hat{\mathbf{1}} + \kappa [(k_x^2 - k_y^2) \hat{\tau}^x + 2k_x k_y \hat{\tau}^y] \} + \frac{\lambda_{\text{soc}}}{2} \hat{\tau}^z \hat{\sigma}^z, \quad (3)$$

where $\hat{\tau}^i$ and $\hat{\sigma}^i$ ($i = x, y, z$) are Pauli matrices acting on orbital and spin, respectively. m^* is the average effective mass, $\kappa = (m_+ - m_-)/(m_+ + m_-)$ is real parameterizing the effective mass ratio of light (m_-) and heavy (m_+) bands at Γ . λ_{soc} is the SOC strength, which lifts the orbital degeneracy and opens up a topological gap at Γ . $V(\mathbf{r})$ is spatially periodic with the periodicity \mathbf{L}_1 and \mathbf{L}_2 , which can be Fourier expanded as

$$V(\mathbf{r}) = V_0 + \sum_{n,i} V(\mathbf{g}_{n,i}) e^{i\mathbf{g}_{n,i} \cdot \mathbf{r}}, \quad (4)$$

where $\mathbf{g}_{n,i}$ denote the six moiré reciprocal lattice vectors $i = 1, 2, 3, 4, 5, 6$ (related via C_6 rotations) to the n -th moiré Brillouin zone, $\mathbf{g}_{n,4} = -\mathbf{g}_{n,1}$, $\mathbf{g}_{n,5} = -\mathbf{g}_{n,2}$, $\mathbf{g}_{n,6} = -\mathbf{g}_{n,3}$. The $h \in C_{6v}$ symmetry $V(\mathbf{r}) = hV(h\mathbf{r})h^{-1}$ and time-reversal \mathcal{T} symmetry $\mathcal{T}^\dagger V(\mathbf{r})\mathcal{T} = V(\mathbf{r})$ lead to $V(\mathbf{g}_{n,1}) = V(\mathbf{g}_{n,4})$, $V(\mathbf{g}_{n,2}) = V(\mathbf{g}_{n,5})$, $V(\mathbf{g}_{n,3}) = V(\mathbf{g}_{n,6})$, and

$$V(\mathbf{g}_{n,1}) = \begin{pmatrix} \alpha_n & \beta_n e^{-i\frac{\pi}{3}} \\ \beta_n e^{i\frac{\pi}{3}} & \alpha_n \end{pmatrix}, V(\mathbf{g}_{n,2}) = \begin{pmatrix} \alpha_n & -\beta_n \\ -\beta_n & \alpha_n \end{pmatrix}, \\ V(\mathbf{g}_{n,3}) = \begin{pmatrix} \alpha_n & \beta_n e^{i\frac{\pi}{3}} \\ \beta_n e^{-i\frac{\pi}{3}} & \alpha_n \end{pmatrix}. \quad (5)$$

Here α_n and β_n parameterizes the Fourier modes of interlayer coupling, and we expect the tunneling decays for higher harmonics [6].

The emergent lattice structure of moiré pattern is explicitly seen by diagonalizing H_{eff} with only $V(\mathbf{r})$ keeping up to second order terms. The parameters $\alpha_{1,2}$ and $\beta_{1,2}$ for realistic materials can be obtained by fitting the band structure from first-principles calculations. Fig. 1 demonstrates the *typical* effective potential of twisted bilayer with C_{6v} symmetry. For example, when $\alpha_{1,2}$ dominate, one get the triangle or honeycomb lattices; when $\beta_{1,2}$ dominates, one get the Kagomé or ruby lattices. As such, the line graph of biparticle lattice emerges and the topological flat band is expected [55]. The effective lattices for twisted bilayer with symmetry groups in Table I are exhaustively calculated in Supplementary Materials. Here we focus on those lattices which enforces the topological flat bands and draw the conclusion: for twisted orbital-active hexagonal bilayer (C_3, C_{3v}, C_6, C_{6v}), honeycomb and Kagomé lattices could emerge, where isolated topological quasiflat bands are obtained in the presence of SOC; while for twisted tetragonal bilayer (C_4, C_{4v}), square and Lieb (as well as line graph of Lieb) lattices could emerge, where the latter is fine tuned, thus flat bands are not guaranteed. Next we predict two candidate materials to realize the salient physics described here.

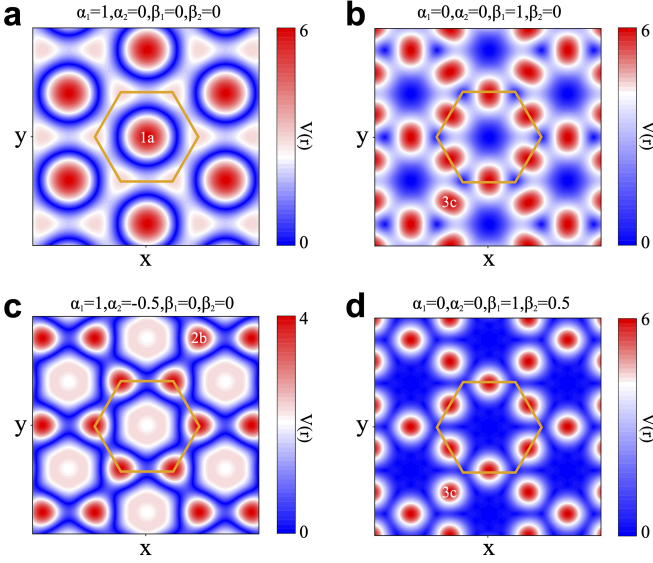


FIG. 1. **Typical effective potentials of twisted bilayer with C_{6v} symmetry.** The relative magnitudes between $\alpha_{1,2}$ and $\beta_{1,2}$ gives rise to different moiré lattice structure at the potential extremum. The maximal 1a, 2b, and 3c Wyckoff positions of a hexagonal lattice are labelled. For example, b, d, Kagomé lattice from the Wyckoff position 3c emerges when $\beta_{1,2}$ dominates.

Materials. PbS_2 is an exfoliable semiconductor, and its monolayer with 2H structure has been introduced in Computational 2D Materials Database (C2DB) [56, 57]. 2H- PbS_2 phase is more stable (total energy 0.47 eV/u.c. lower) than its 1T phase. The band structure of monolayer 2H- PbS_2 without SOC from first-principles calculations is shown in Fig. 2a. In contrast to group-VI TMD such as MoS_2 with 2H structure, the valence band maximum in 2H- PbS_2 is located at Γ , and without SOC it is characterized by two-fold degenerate chalcogen p_x, p_y orbitals enforced by space group $P\bar{6}m2$. The atomic SOC lifts the degeneracy and introduces a gap of about 65 meV. The parameters in Eq. (3) are obtained from first-principles calculations $m^* = 0.7m_0$, with m_0 the mass of free electron, $\kappa = 0.9$, and $\lambda_{\text{soc}} = 65$ meV. The parameters in $V(\mathbf{r})$ up to second order are obtained by fitting the *ab initio* band structures with different stacking configurations such as AA, AB, X and Y shown in Fig. 2b, $\alpha_1 = -24.3$ meV, $\alpha_2 = 5.5$ meV, $\beta_1 = 26.8$ meV, and $\beta_2 = 10.3$ meV. The band structure from the continuum model and DFT calculations for twisted bilayer of 6° without SOC matches well with each other in Fig. 2c, justifying the validity of the fitted parameters.

The band structures for valence electrons calculated in Fig. 2c show clearly the emergent Kagomé flat bands. To reveal the nature of moiré band physics, we identify the symmetries and centers of the Wannier orbitals underlying the moiré bands. The wave function density distribution of the three selected Bloch states that are

circled in Fig. 2c is generated by orbitals centered on a Kagomé lattice shown in Fig. 2d. The SOC lifts the degeneracy at Γ , and the flat band is gapped from other dispersive band which becomes quasiflat and is topological with spin Chern number $C_s = \pm 1$. The flatness of the top-most topological band is insensitive to the twist angle since they come from the interference effect.

CdS is another exfoliable semiconductor, and its monolayer has been introduced in 2D Materials Encyclopedia [58]. The band structure of monolayer CdS without SOC from DFT calculations is shown in Fig. 3a. Similar to monolayer 2H- PbS_2 , the valence band maximum of monolayer CdS is located at Γ , which is composed of two-fold degenerate chalcogen p_x, p_y orbitals enforced by space group $P3m1$. The atomic SOC lifts the degeneracy and introduces a gap of about 14 meV. The parameters for CdS in Eq. (3) are obtained from DFT calculations $m^* = 0.9m_0$, $\kappa = 0.9$ and $\lambda_{\text{soc}} = 13.4$ meV. The parameters in $V(\mathbf{r})$ are fitted with the *ab initio* band structures as $\alpha_1 = -45.6$ meV, $\alpha_2 = 41.5$ meV, $\beta_1 = 16.5$ meV, and $\beta_2 = 7$ meV.

The band structures for valence electron calculated in Fig. 3c show the emergent honeycomb flat bands with degenerate p_x, p_y orbitals near the Fermi level by employing topological quantum chemistry [59, 60]. The charge density distribution of the selected Bloch states circled in Fig. 3c is generated by multiorbitals centered on a honeycomb lattice shown in Fig. 3d. Such emergent honeycomb lattice can be explained by the maximum of $V(\mathbf{r})$ dominated by $\alpha_{1,2}$. The SOC lifts the degeneracy at Γ and gap the flat band with spin Chern number $C_s = \pm 1$. The salient low-energy physics of orbital-active biparticle lattice is quite unusual, since it is not energetically favorable in 2D crystalline materials for p_x, p_y orbitals such as graphene due to sp^2 configuration. It is worth mentioning that the band structure for twist angle 4° looks like the Kane-Mele type [61], because now λ_{soc} becomes the dominate energy scale and splits the degenerate p_x, p_y orbitals into $p_{\pm} = p_x \pm ip_y$, as such the low-energy physics is characterized by single orbital.

Superfluid weight and BKT transition. The tunable realization of isolated topological flat bands in twisted orbital-active bilayer provides an ideal platform for hosting correlated topological phases, including fractional quantum anomalous Hall effect [62–68] and unconventional superconductivity [2, 8]. Here we study superconductivity of twisted bilayer PbS_2 and CdS with local attractive interactions. We obtain the superfluid weight and Berezinskii-Kosterlitz-Thouless (BKT) transition temperature for low-energy continuum and tight-binding models.

We consider the local attractive interaction $H_{\text{int}} = -g \int d\mathbf{r} \psi_{l\tau\uparrow}^\dagger \psi_{l'\tau'\downarrow}^\dagger \psi_{l'\tau'\downarrow} \psi_{l\tau\uparrow}$, where l denotes layer and τ denotes orbital degrees of freedom. The local interaction has been used to study s -wave superconductivity, mediated by electron-phonon interaction in twisted bi-

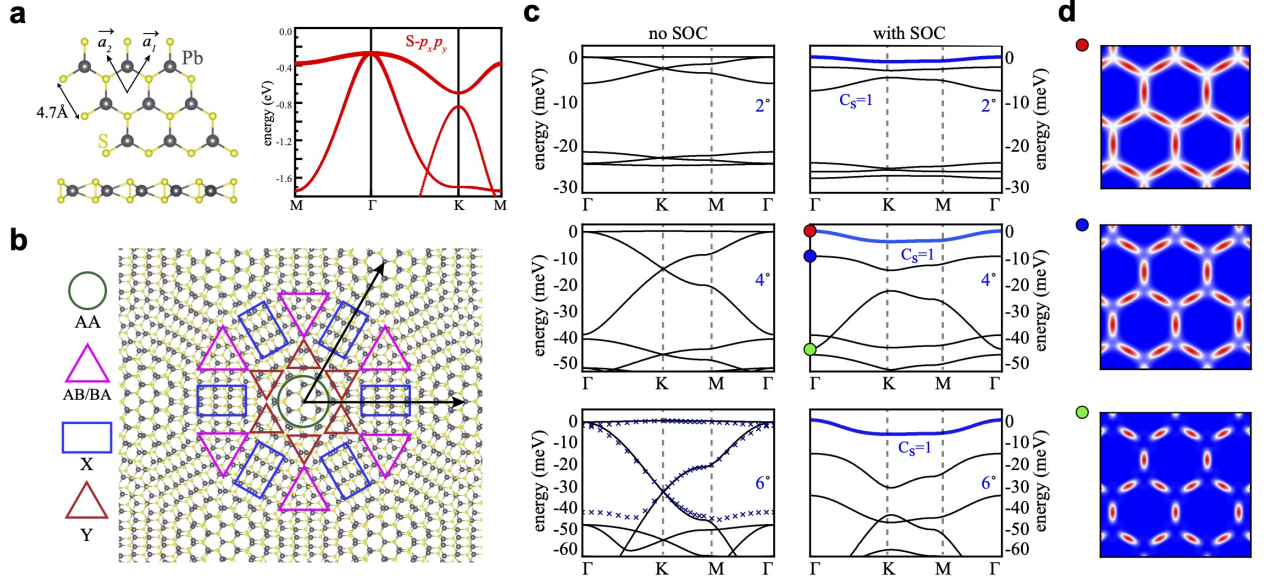


FIG. 2. **Moiré pattern and topological flat bands in twisted PbS₂ bilayer.** **a**, Crystal structure and electronic structure without SOC of monolayer 2H-PbS₂, the in-plane lattice vectors \mathbf{a}_1 and \mathbf{a}_2 are shown. **b**, In the small angle twisted PbS₂ bilayer, the interlayer stacking has AA, AB/BA, X and Y in the moiré unit cell, where $\mathbf{t}_{AA}(\mathbf{r}) = 0$, $\mathbf{t}_{AB/BA}(\mathbf{r}) = \pm(\mathbf{a}_1 + \mathbf{a}_2)/3$, $\mathbf{t}_X(\mathbf{r}) = (\mathbf{a}_1 + \mathbf{a}_2)/2$, and $\mathbf{t}_Y(\mathbf{r}) = (\mathbf{a}_1 + \mathbf{a}_2)/6$. **c**, The band structure of twisted bilayers from continuum model for three representative twist angles without (left column) and with (right column) SOC. The top-most valence bands demonstrate the flat bands on the emergent Kagomé lattice. The SOC lifts the quadratic band touching of Kagomé bands at Γ and leads to isolated topological quasiflat bands (blue lines) with spin Chern number $C_s = \pm 1$. For twist angle 6° without SOC, the band structure from continuum model matches well with that from first-principles calculations (navy cross). **d**, The wave function density distribution of the three selected Bloch states that are circled in **c**, which clearly shows the emergent Kagomé lattice.

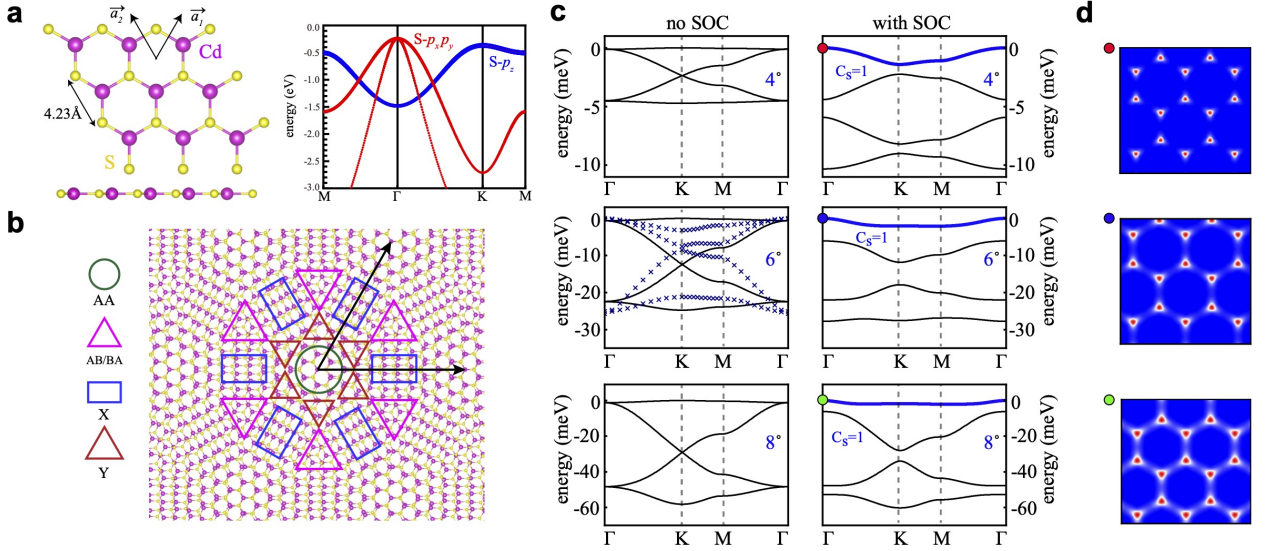


FIG. 3. **Moiré pattern and topological flat bands in twisted CdS bilayer.** **a**, Top and side view of crystal structure of monolayer CdS, where the in-plane lattice vectors \mathbf{a}_1 and \mathbf{a}_2 are shown. The electronic structure without SOC from DFT calculation. **b**, In the small angle twisted CdS bilayer, the interlayer stacking has AA, AB/BA, X and Y in the moiré unit cell. Here $\mathbf{t}_{AA}(\mathbf{r}) = 0$, $\mathbf{t}_{AB/BA}(\mathbf{r}) = \pm(\mathbf{a}_1 + \mathbf{a}_2)/3$, $\mathbf{t}_X(\mathbf{r}) = (\mathbf{a}_1 + \mathbf{a}_2)/2$, and $\mathbf{t}_Y(\mathbf{r}) = (\mathbf{a}_1 + \mathbf{a}_2)/6$. **c**, The band structure of twisted bilayers from continuum model for three representative twist angles without (left column) and with (right column) SOC. The top-most valence bands demonstrate the flat bands on the emergent honeycomb lattice. The SOC lifts the quadratic band touching of honeycomb bands at Γ and leads to isolated topological quasiflat bands (blue lines) with spin Chern number $C_s = \pm 1$. For twist angle 6° without SOC, the band structure from continuum model qualitatively matches well with that from DFT calculations (navy cross). **d**, The wave function density distribution of the three selected Bloch states that are circled in **c**, which clearly shows the emergent honeycomb lattice.

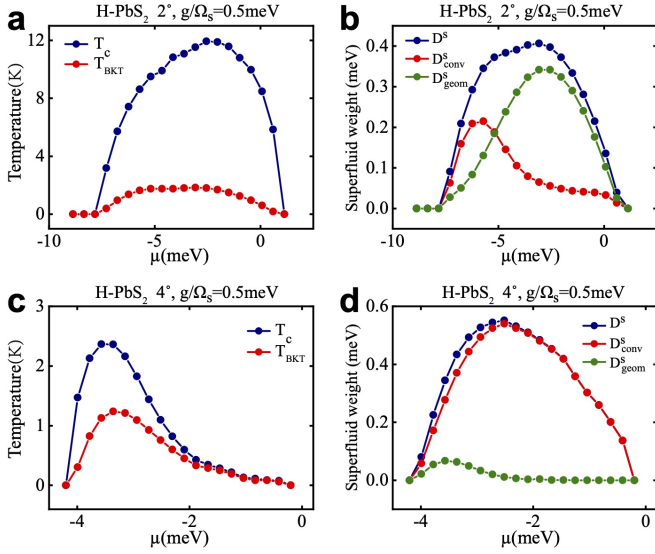


FIG. 4. **Superfluid weight and BKT temperature.** **a,c,** The critical temperature and BKT temperature as a function of chemical potential for Kagomé bands in twisted PbS₂ bilayer of 2° and 4°, respectively. **b,d,** The corresponding various components of superfluid weight.

layer graphene [69, 70]. Now the total Hamiltonian is $\mathcal{H} = H_{\text{eff}} - \mu N + H_{\text{int}}$, where N is particle number operator and μ is the chemical potential. To determine the superfluid weight D^s , we first solve the order parameters from the BCS gap equation. After projecting the interaction term onto bands near the Fermi surface by $\psi_{l\tau\sigma}(\mathbf{k} + \mathbf{G}) = \sum_n u_{n\sigma\mathbf{G}}(l, \tau, \mathbf{k}) c_{n\sigma}(\mathbf{k})$, where $u_{n\sigma}(\mathbf{k})$ is the Bloch wave function and $c_{n\sigma}(\mathbf{k})$ is the annihilation operator with band index n , spin σ and reciprocal vector \mathbf{G} , the interacting Hamiltonian is solved by mean field approximation with order parameter matrix as $\Delta(\mathbf{k})_{n_3, n_4} = (1/A) \sum_{\mathbf{k}_1} [V_{\mathbf{k}, -\mathbf{k}, \mathbf{k}_1 - \mathbf{k}}]_{n_2, n_3}^{n_1, n_4} \langle c_{n_1, \uparrow}^\dagger(\mathbf{k}_1) c_{n_2, \downarrow}^\dagger(-\mathbf{k}_1) \rangle$. We solve the linearized gap equation to obtain the leading pairing instability and the critical temperature T_c as

$$\Delta^\dagger(\mathbf{k}_1)_{n_1, n_2} = \frac{1}{A} \sum_{\mathbf{k}} [V_{\mathbf{k}, -\mathbf{k}, \mathbf{k}_1 - \mathbf{k}}]_{n_2, n_3}^{n_1, n_4} f_{F, n_4, n_3}(\mathbf{k}) \Delta^\dagger(\mathbf{k})_{n_4, n_3}, \quad (6)$$

where $f_{F, n_1, n_2} = \frac{1 - n_F(\varepsilon_{n_1, \uparrow}) - n_F(\varepsilon_{n_2, \downarrow})}{\varepsilon_{n_1, \uparrow} + \varepsilon_{n_2, \downarrow}}$ and $[V_{\mathbf{k}, \mathbf{k}_1, \mathbf{q}}]_{n_2, n_3}^{n_1, n_4} = g \sum_{\mathbf{G}} \Lambda_{\mathbf{q} + \mathbf{G}, \uparrow}^{n_1, n_4}(\mathbf{k}) \Lambda_{-\mathbf{q} - \mathbf{G}, \downarrow}^{n_2, n_3}(\mathbf{k}_1)$, A is area of the sample, n_F is the Fermi-Dirac distribution and $\varepsilon_{n, \sigma}$ is the band dispersion, $\Lambda_{\mathbf{q} + \mathbf{G}, \sigma}^{n_1, n_2}(\mathbf{k}) = \langle u_{n_1 \sigma}, \mathbf{k} + \mathbf{q} + \mathbf{G} | u_{n_2 \sigma}, \mathbf{k} \rangle$. The maximum of order parameter depends almost linearly on g , which is typical for generic flat band systems. Here we choose $g/\Omega_s = 0.5$ meV based on previous studies on electron-phonon coupling in moiré system [69, 70], where Ω_s is the area of the moiré unit cell. The accurate strength relies on microscopic details of electron-phonon coupling, which is beyond the scope of this paper.

As the system is two-dimensional, the transition to

superconductivity is bound to occur at the BKT temperature T_{BKT} [71–73], which can be determined from $k_B T_{\text{BKT}} = (\pi/8) \sqrt{\det(D^s(T_{\text{BKT}}))}$. From the linear response theory, D^s is the zero-frequency, long-wavelength limit of the current-current response function $D_{\mu\nu}^s = \lim_{\mathbf{q} \rightarrow 0} [\lim_{\omega \rightarrow 0} K_{\mu\nu}(\mathbf{q}, \omega)]$ [74], where $\mu, \nu \in (x, y)$. The local attractive interaction, yielding the spin-singlet s -wave pairing, conserves the underlying C_3 rotational symmetry of the twisted bilayer lattices which enforces D^s to be isotropic, i.e., $D_{xx}^s = D_{yy}^s$ and $D_{xy}^s = D_{yx}^s = 0$. Fig. 4c and 4d depict the numerical results of T_{BKT} and D^s for twisted PbS₂ bilayer at twisting angle $\theta = 4^\circ$. Since the band width and interband gaps are greater than the interaction strength, we could only keep the Kagomé bands. As we can see, T_c follows the density of state as in the BCS superconductor, and the superfluid weight is dominated by the conventional part D_{conv}^s which is proportional to the group velocity of electronic bands around the Fermi level. $D^s = D_{\text{conv}}^s + D_{\text{geom}}^s$, where D_{geom}^s is a multiband effect depending on the overlap of the Bloch states and their momentum derivatives. When the twist angle further decreases to $\theta = 2^\circ$, the band widths become much smaller as shown in Fig. 2c. The reduced band width indicates the more localized wannier orbitals in real space, thus the Hamiltonian reduces to Kagomé lattice attractive Hubbard model with Hubbard $|U|$ comparable with the band width. As depicted in Fig. 4a and 4b, the increased $|U|$ and density of state are reflected in relatively large T_c , and large proportion of the superfluid weight comes from geometric part when the chemical potential enters flat band. All these features were verified for the lattice model calculation in Supplementary Materials.

Discussion. The moiré engineering of twisted orbital-active bilayer leads to interesting and unique topological electronic structure. Besides the superconductivity, the realization of isolated topological flat bands here further provides a promising and tunable platform to realize a variety of correlated topological states of matter, including fractional topological insulator and fractional quantum anomalous Hall effect. The guiding principle for searching realistic materials is to find hexagonal lattice with minimal C_3 symmetry, where the low-energy physics is at Γ . Therefore stronger band flattening at larger twist angles in the quadratic cases is expected comparing with the linear cases. All of these requirements are quite common for valence electrons in semiconductors, for example, PbSe₂, SnS₂, SnSe₂, SnTe₂, CdSe, CdTe, ZnSe, etc [56, 57]. Interestingly, the emergent Kagomé lattice could be extended to magnetic moiré systems, which is left for future work.

This work is supported by the National Key Research Program of China under Grant No. 2019YFA0308404, the Natural Science Foundation of China through Grant No. 12174066, Science and Technology Commission of Shanghai Municipality under Grant No. 20JC1415900,

the Innovation Program for Quantum Science and Technology through Grant No. 2021ZD0302600, Shanghai Municipal Science and Technology Major Project under Grant No. 2019SHZDZX01. H.W. and Y.J. contributed equally to this work.

* wjingphys@fudan.edu.cn

- [1] Eva Y. Andrei and Allan H. MacDonald, “Graphene bilayers with a twist,” *Nature Mat.* **19**, 1265 (2020).
- [2] Leon Balents, Cory R. Dean, Dmitri K. Efetov, and Andrea F. Young, “Superconductivity and strong correlations in moiré flat bands,” *Nature Phys.* **16**, 725 (2020).
- [3] Stephen Carr, Shiang Fang, and Efthimios Kaxiras, “Electronic-structure methods for twisted moiré layers,” *Nature Rev. Mater.* **5**, 748 (2020).
- [4] Dante M. Kennes, Martin Claassen, Lede Xian, Antoine Georges, Andrew J. Millis, James Hone, Cory R. Dean, D. N. Basov, Abhay N. Pasupathy, and Angel Rubio, “Moiré heterostructures as a condensed-matter quantum simulator,” *Nature Phys.* **17**, 155–163 (2021).
- [5] Eva Y. Andrei, Dmitri K. Efetov, Pablo Jarillo-Herrero, Allan H. MacDonald, Kin Fai Mak, T. Senthil, Emanuel Tutuc, Ali Yazdani, and Andrea F. Young, “The marvels of moiré materials,” *Nature Rev. Mater.* **6**, 201–206 (2021).
- [6] R. Bistritzer and A. H. MacDonald, “Moiré bands in twisted double-layer graphene,” *Proc. Natl. Acad. Sci. U.S.A.* **108**, 12233–12237 (2011).
- [7] Yuan Cao, Valla Fatemi, Ahmet Demir, Shiang Fang, Spencer L. Tomarken, Jason Y. Luo, Javier D. Sanchez-Yamagishi, Kenji Watanabe, Takashi Taniguchi, Efthimios Kaxiras, Ray C. Ashoori, and Pablo Jarillo-Herrero, “Correlated insulator behaviour at half-filling in magic-angle graphene superlattices,” *Nature* **556**, 80–84 (2018).
- [8] Y. Cao, V. Fatemi, S. Fang, K. Watanabe, T. Taniguchi, E. Kaxiras, and P. Jarillo-Herrero, “Unconventional superconductivity in magic-angle graphene superlattices,” *Nature* **556**, 43 (2018).
- [9] M. Yankowitz, S. Chen, H. Polshyn, Y. Zhang, K. Watanabe, T. Taniguchi, D. Graf, A. F. Young, and C. R. Dean, “Tuning superconductivity in twisted bilayer graphene,” *Science* **363**, 1059–1064 (2019).
- [10] Xiaobo Lu, Petr Stepanov, Wei Yang, Ming Xie, Mohammed Ali Aamir, Ipsita Das, Carles Urgell, Kenji Watanabe, Takashi Taniguchi, Guangyu Zhang, Adrian Bachtold, Allan H. MacDonald, and Dmitri K. Efetov, “Superconductors, orbital magnets and correlated states in magic-angle bilayer graphene,” *Nature* **574**, 653–657 (2019).
- [11] A. L. Sharpe, E. J. Fox, A. W. Barnard, J. Finney, K. Watanabe, T. Taniguchi, M. A. Kastner, and D. Goldhaber-Gordon, “Emergent ferromagnetism near three-quarters filling in twisted bilayer graphene,” *Science* **365**, 605–608 (2019).
- [12] G. Chen, A. L. Sharpe, P. Gallagher, I. T. Rosen, E. J. Fox, L. Jiang, B. Lyu, H. Li, K. Watanabe, T. Taniguchi, J. Jung, Z. Shi, D. Goldhaber-Gordon, Y. Zhang, and F. Wang, “Signatures of tunable superconductivity in a trilayer graphene moiré superlattice,” *Nature* **572**, 215–219 (2019).
- [13] Xiaomeng Liu, Zeyu Hao, Eslam Khalaf, Jong Yeon Lee, Yuval Ronen, Hyobin Yoo, Danial Haei Najafabadi, Kenji Watanabe, Takashi Taniguchi, Ashvin Vishwanath, and Philip Kim, “Tunable spin-polarized correlated states in twisted double bilayer graphene,” *Nature* **583**, 221–225 (2020).
- [14] M. Serlin, C. L. Tschirhart, H. Polshyn, Y. Zhang, J. Zhu, K. Watanabe, T. Taniguchi, L. Balents, and A. F. Young, “Intrinsic quantized anomalous hall effect in a moiré heterostructure,” *Science* **367**, 900–903 (2020).
- [15] Petr Stepanov, Ipsita Das, Xiaobo Lu, Ali Fahimniya, Kenji Watanabe, Takashi Taniguchi, Frank H. L. Koppens, Johannes Lischner, Leonid Levitov, and Dmitri K. Efetov, “Untying the insulating and superconducting orders in magic-angle graphene,” *Nature* **583**, 375–378 (2020).
- [16] Yuan Cao, Debanjan Chowdhury, Daniel Rodan-Legrain, Oriol Rubies-Bigorda, Kenji Watanabe, Takashi Taniguchi, T. Senthil, and Pablo Jarillo-Herrero, “Strange metal in magic-angle graphene with near planckian dissipation,” *Phys. Rev. Lett.* **124**, 076801 (2020).
- [17] Yuan Cao, Daniel Rodan-Legrain, Jeong Min Park, Noah F. Q. Yuan, Kenji Watanabe, Takashi Taniguchi, Rafael M. Fernandes, Liang Fu, and Pablo Jarillo-Herrero, “Nematicity and competing orders in superconducting magic-angle graphene,” *Science* **372**, 264–271 (2021).
- [18] Tingxin Li, Shengwei Jiang, Bowen Shen, Yang Zhang, Lizhong Li, Zui Tao, Trithep Devakul, Kenji Watanabe, Takashi Taniguchi, Liang Fu, Jie Shan, and Kin Fai Mak, “Quantum anomalous hall effect from intertwined moiré bands,” *Nature* **600**, 641–646 (2021).
- [19] Yang Zhang, Trithep Devakul, and Liang Fu, “Spin-textured chern bands in ab-stacked transition metal dichalcogenide bilayers,” *Pro. Natl. Acad. Sci.* **118**, e2112673118 (2021).
- [20] Ying-Ming Xie, Cheng-Ping Zhang, Jin-Xin Hu, Kin Fai Mak, and K. T. Law, “Valley-polarized quantum anomalous hall state in moiré $\text{mote}_2/\text{wse}_2$ heterobilayers,” *Phys. Rev. Lett.* **128**, 026402 (2022).
- [21] J. Kang and O. Vafek, “Strong coupling phases of partially filled twisted bilayer graphene narrow bands,” *Phys. Rev. Lett.* **122**, 246401 (2019).
- [22] A. Kerelsky, L. J. McGilly, D. M. Kennes, L. Xian, M. Yankowitz, S. Chen, K. Watanabe, T. Taniguchi, J. Hone, C. Dean, A. Rubio, and A. N. Pasupathy, “Maximized electron interactions at the magic angle in twisted bilayer graphene,” *Nature* **572**, 95 (2019).
- [23] Yonglong Xie, Biao Lian, Berthold Jack, Xiaomeng Liu, Cheng-Li Chiu, Kenji Watanabe, Takashi Taniguchi, B. Andrei Bernevig, and Ali Yazdani, “Spectroscopic signatures of many-body correlations in magic-angle twisted bilayer graphene,” *Nature* **572**, 101–105 (2019).
- [24] Biao Lian, Zhi-Da Song, Nicolas Regnault, Dmitri K. Efetov, Ali Yazdani, and B. Andrei Bernevig, “Twisted bilayer graphene. iv. exact insulator ground states and phase diagram,” *Phys. Rev. B* **103**, 205414 (2021).
- [25] Sebastiano Peotta and Päivi Törmä, “Superfluidity in topologically nontrivial flat bands,” *Nature Commun.* **6**, 1–9 (2015).
- [26] Xiang Hu, Timo Hyart, Dmitry I. Pikulin, and Enrico Rossi, “Geometric and conventional contribution to

- the superfluid weight in twisted bilayer graphene,” *Phys. Rev. Lett.* **123**, 237002 (2019).
- [27] A. Julku, T. J. Peltonen, L. Liang, T. T. Heikkilä, and P. Törmä, “Superfluid weight and berezinskii-kosterlitz-thouless transition temperature of twisted bilayer graphene,” *Phys. Rev. B* **101**, 060505 (2020).
- [28] Fang Xie, Zhida Song, Biao Lian, and B. Andrei Bernevig, “Topology-bounded superfluid weight in twisted bilayer graphene,” *Phys. Rev. Lett.* **124**, 167002 (2020).
- [29] Jonah Herzog-Arbeitman, Valerio Peri, Frank Schindler, Sebastian D. Huber, and B. Andrei Bernevig, “Superfluid weight bounds from symmetry and quantum geometry in flat bands,” *Phys. Rev. Lett.* **128**, 087002 (2022).
- [30] Päivi Törmä, Sebastiano Peotta, and Bogdan A Bernevig, “Superfluidity and quantum geometry in twisted multilayer systems,” *arXiv: 2111.00807* (2021), 10.48550/arXiv.2111.00807.
- [31] Valerio Peri, Zhi-Da Song, B. Andrei Bernevig, and Sebastian D. Huber, “Fragile topology and flat-band superconductivity in the strong-coupling regime,” *Phys. Rev. Lett.* **126**, 027002 (2021).
- [32] Nishchhal Verma, Tamaghna Hazra, and Mohit Randeria, “Optical spectral weight, phase stiffness, and t_c bounds for trivial and topological flat band superconductors,” *Proc. Natl. Acad. Sci. U.S.A.* **118**, e2106744118 (2021).
- [33] Nicola Marzari, Arash A. Mostofi, Jonathan R. Yates, Ivo Souza, and David Vanderbilt, “Maximally localized wannier functions: Theory and applications,” *Rev. Mod. Phys.* **84**, 1419–1475 (2012).
- [34] N. B. Kopnin, T. T. Heikkilä, and G. E. Volovik, “High-temperature surface superconductivity in topological flat-band systems,” *Phys. Rev. B* **83**, 220503 (2011).
- [35] Xiao-Liang Qi and Shou-Cheng Zhang, “Topological insulators and superconductors,” *Rev. Mod. Phys.* **83**, 1057–1110 (2011).
- [36] Masatoshi Sato and Yoichi Ando, “Topological superconductors: a review,” *Rep. Prog. Phys.* **80**, 076501 (2017).
- [37] A Mielke, “Ferromagnetic ground states for the hubbard model on line graphs,” *J. Phys. A* **24**, L73–L77 (1991).
- [38] A Mielke, “Ferromagnetism in the hubbard model on line graphs and further considerations,” *J. Phys. A* **24**, 3311–3321 (1991).
- [39] Hal Tasaki, “From Nagaoka’s Ferromagnetism to Flat-Band Ferromagnetism and Beyond: An Introduction to Ferromagnetism in the Hubbard Model,” *Prog. Theor. Phys.* **99**, 489–548 (1998).
- [40] Congjun Wu, Doron Bergman, Leon Balents, and S. Das Sarma, “Flat bands and wigner crystallization in the honeycomb optical lattice,” *Phys. Rev. Lett.* **99**, 070401 (2007).
- [41] Doron L. Bergman, Congjun Wu, and Leon Balents, “Band touching from real-space topology in frustrated hopping models,” *Phys. Rev. B* **78**, 125104 (2008).
- [42] Zheng Liu, Feng Liu, and Yong-Shi Wu, “Exotic electronic states in the world of flat bands: From theory to material,” *Chin. Phys. B* **23**, 077308 (2014).
- [43] Da-Shuai Ma, Yuanfeng Xu, Christie S. Chiu, Nicolas Regnault, Andrew A. Houck, Zhida Song, and B. Andrei Bernevig, “Spin-orbit-induced topological flat bands in line and split graphs of bipartite lattices,” *Phys. Rev. Lett.* **125**, 266403 (2020).
- [44] Dumitru Călugăru, Aaron Chew, Luis Elcoro, Yuanfeng Xu, Nicolas Regnault, Zhi-Da Song, and B. Andrei Bernevig, “General construction and topological classification of crystalline flat bands,” *Nature Phys.* **18**, 185–189 (2022).
- [45] Nicolas Regnault, Yuanfeng Xu, Ming-Rui Li, Da-Shuai Ma, Milena Jovanovic, Ali Yazdani, Stuart S. P. Parkin, Claudia Felser, Leslie M. Schoop, N. Phuan Ong, Robert J. Cava, Luis Elcoro, Zhi-Da Song, and B. Andrei Bernevig, “Catalogue of flat-band stoichiometric materials,” *Nature* **603**, 824–828 (2022).
- [46] Hang Liu, Sheng Meng, and Feng Liu, “Screening two-dimensional materials with topological flat bands,” *Phys. Rev. Materials* **5**, 084203 (2021).
- [47] Mattia Angeli and Allan H MacDonald, “ γ valley transition metal dichalcogenide moiré bands,” *Proc. Natl. Acad. Sci. U.S.A.* **118**, e2021826118 (2021).
- [48] Ding Pei, Binbin Wang, Zishu Zhou, Zhihai He, Liheng An, Shanmei He, Cheng Chen, Yiwei Li, Liyang Wei, Aiji Liang, Jose Avila, Pavel Dudin, Viktor Kandyba, Alessio Giampietri, Mattia Cattelan, Alexei Barinov, Zhongkai Liu, Jianpeng Liu, Hongming Weng, Ning Wang, Jiamin Xue, and Yulin Chen, “Observation of Γ -valley moiré bands and emergent hexagonal lattice in twisted transition metal dichalcogenides,” *Phys. Rev. X* **12**, 021065 (2022).
- [49] Zhaochen Liu, Huan Wang, and Jing Wang, “Magnetic moiré surface states and flat chern bands in topological insulators,” *Phys. Rev. B* **106**, 035114 (2022).
- [50] Biao Lian, Zhaochen Liu, Yuanbo Zhang, and Jing Wang, “Flat chern band from twisted bilayer mnbi_2te_4 ,” *Phys. Rev. Lett.* **124**, 126402 (2020).
- [51] Jeil Jung, Arnaud Raoux, Zhenhua Qiao, and A. H. MacDonald, “Ab initio theory of moiré superlattice bands in layered two-dimensional materials,” *Phys. Rev. B* **89**, 205414 (2014).
- [52] F. Wu, T. Lovorn, E. Tutuc, I. Martin, and A. H. MacDonald, “Topological insulators in twisted transition metal dichalcogenide homobilayers,” *Phys. Rev. Lett.* **122**, 086402 (2019).
- [53] Toshikaze Kariyado and Ashvin Vishwanath, “Flat band in twisted bilayer bravais lattices,” *Phys. Rev. Research* **1**, 033076 (2019).
- [54] Leon Balents, “General continuum model for twisted bilayer graphene and arbitrary smooth deformations,” *SciPost Phys.* **7**, 48 (2019).
- [55] Huan Wang and Jing Wang, “Topological bands in two-dimensional orbital-active bipartite lattices,” *Phys. Rev. B* **103**, L081109 (2021).
- [56] Sten Haastrup, Mikkel Strange, Mohnish Pandey, Thorsten Deilmann, Per S Schmidt, Nicki F Hinsche, Morten N Gjerding, Daniele Torelli, Peter M Larsen, Anders C Riis-Jensen, Jakob Gath, Karsten W Jacobsen, Jens Jørgen Mortensen, Thomas Olsen, and Kristian S Thygesen, “The computational 2d materials database: high-throughput modeling and discovery of atomically thin crystals,” *2D Mater.* **5**, 042002 (2018).
- [57] Morten Niklas Gjerding, Alireza Taghizadeh, Asbjørn Rasmussen, Sajid Ali, Fabian Bertoldo, Thorsten Deilmann, Nikolaj Rørbye Knøsgaard, Mads Kruse, Ask Hjorth Larsen, Simone Manti, Thomas Garm Pedersen, Urko Petralanda, Thorbjørn Skovhus, Mark Kamper Svendsen, Jens Jørgen Mortensen, Thomas Olsen, and Kristian Sommer Thygesen, “Recent progress of the computational 2d materials database (c2db),” *2D Mater* **8**,

- 044002 (2021).
- [58] Jun Zhou, Lei Shen, Miguel Dias Costa, Kristin A Persson, Shyue Ping Ong, Patrick Huck, Yunhao Lu, Xiaoyang Ma, Yiming Chen, Hanmei Tang, *et al.*, “2dmatpedia, an open computational database of two-dimensional materials from top-down and bottom-up approaches,” *Sci. data* **6**, 1–10 (2019).
 - [59] Barry Bradlyn, L Elcoro, Jennifer Cano, MG Vergniory, Zhijun Wang, C Felser, MI Aroyo, and B Andrei Bernevig, “Topological quantum chemistry,” *Nature* **547**, 298 (2017).
 - [60] Jorrit Kruthoff, Jan de Boer, Jasper van Wezel, Charles L. Kane, and Robert-Jan Slager, “Topological classification of crystalline insulators through band structure combinatorics,” *Phys. Rev. X* **7**, 041069 (2017).
 - [61] C. L. Kane and E. J. Mele, “Quantum Spin Hall Effect in Graphene,” *Phys. Rev. Lett.* **95**, 226801 (2005).
 - [62] M. Levin and A. Stern, “Fractional topological insulators,” *Phys. Rev. Lett.* **103**, 196803 (2009).
 - [63] J. Maciejko, X.-L. Qi, A. Karch, and S.-C. Zhang, “Fractional topological insulators in three dimensions,” *Phys. Rev. Lett.* **105**, 246809 (2010).
 - [64] X.-L. Qi, “Generic wave-function description of fractional quantum anomalous hall states and fractional topological insulators,” *Phys. Rev. Lett.* **107**, 126803 (2011).
 - [65] E. Tang, J.-W. Mei, and X.-G. Wen, “High-temperature fractional quantum hall states,” *Phys. Rev. Lett.* **106**, 236802 (2011).
 - [66] K. Sun, Z. Gu, H. Katsura, and S. Das Sarma, “Nearly flatbands with nontrivial topology,” *Phys. Rev. Lett.* **106**, 236803 (2011).
 - [67] T. Neupert, L. Santos, C. Chamon, and C. Mudry, “Fractional quantum hall states at zero magnetic field,” *Phys. Rev. Lett.* **106**, 236804 (2011).
 - [68] Martin Claassen, Lede Xian, Dante M. Kennes, and Angel Rubio, “Ultra-strong spin-orbit coupling and topological moiré engineering in twisted zrS_2 bilayers,” *Nat. Commun.* **13**, 4915 (2022).
 - [69] Fengcheng Wu, A. H. MacDonald, and Ivar Martin, “Theory of phonon-mediated superconductivity in twisted bilayer graphene,” *Phys. Rev. Lett.* **121**, 257001 (2018).
 - [70] Biao Lian, Zhijun Wang, and B. Andrei Bernevig, “Twisted bilayer graphene: A phonon-driven superconductor,” *Phys. Rev. Lett.* **122**, 257002 (2019).
 - [71] V. L. Berezinsky, “Destruction of long-range order in one-dimensional and two-dimensional systems having a continuous symmetry group i. classical systems,” *Sov. Phys. JETP* **32**, 493–500 (1971).
 - [72] J M Kosterlitz and D J Thouless, “Long range order and metastability in two dimensional solids and superfluids. (application of dislocation theory),” *J. Phys. C* **5**, L124–L126 (1972).
 - [73] J M Kosterlitz and D J Thouless, “Ordering, metastability and phase transitions in two-dimensional systems,” *J. Phys. C* **6**, 1181–1203 (1973).
 - [74] Long Liang, Tuomas I. Vanhala, Sebastiano Peotta, Topi Siro, Ari Harju, and Päivi Törmä, “Band geometry, berry curvature, and superfluid weight,” *Phys. Rev. B* **95**, 024515 (2017).